The paper was published in the proceedings of the 11th International Conference on Physical Modelling in Geotechnics (ICPMG2026) and was edited by Ioannis Anastasopoulos. The conference was held from June 8th to June 12th 2026 in Zurich, Switzerland.

ICPMG 2026

Proceedings of the 11th ICPMG 2026
11th International Conference on Physical Modelling in Geotechnics
8-12 June 2026, Zurich, Switzerland

Experimental verification of installation and bearing capacity of vibro-driven steel pipe piles in a centrifuge

H. Oguma, J. Miyamoto, T. Sato & K. Tsurugasaki
Technical Research Institute, Toyo Construction Co., Ltd., Nishinomiya, Japan,

ooguma-hiroki@toyo-const.co.jp, miyamoto-junji13@toyo-const.co.jp, sato-tomoya@toyo-const.co.jp, tsurugasaki-kazuhiro@toyo-const.co.jp

ABSTRACT: This study examines the bearing capacity of steel pipe piles installed by both vibro-driven and static penetration methods in centrifugal fields and 1g. A series of model tests was conducted using a beam-type centrifuge apparatus at 20g to replicate realistic stress conditions. Brass model piles were penetrated into densely compacted mixed silica sand, and penetration resistance as well as dry density of the soil inside each pile were measured. Results indicated that penetration resistance was 1.5 to 2.0 times higher in centrifugal conditions pile installation compared to 1g fields, and this increase correlated with greater dry density and clogging of the sand within the pile. The measured penetration resistance under 20g was close to values predicted by classical bearing capacity theory, suggesting the centrifuge method is effective for evaluating full-scale pile performance. A comparison of vibro and static penetration methods revealed that vibro penetration led to lower resistance in the early stages due to soil disturbance by vibration. However, at greater depths where vibration effects diminished, penetration resistance became nearly identical for both methods.

1 INTRODUCTION

Steel pipe piles are frequently used as foundation piles for port structures in Japan due to their favorable constructability. These piles are typically employed as open-ended piles, wherein soil clogging at the pile tip enables the entire cross section of the steel pipe to act as bearing resistance, thereby ensuring sufficient end bearing capacity. In recent years, the trend towards larger facilities has led to an increasing adoption of large-diameter steel pipe piles, which are expected to provide greater bearing capacities (Fetrati et al., 2025).

Regarding the pile installation method, the vibro-driven method has become prevalent in recent years due to its advantages in constructability and reduced noise and vibration during installation. Several technical guidelines (e.g., Vibro Hammer Method Technology Study Group, 2024) suggest that the bearing capacity of steel pipe piles installed by the vibro-driven method should be estimated lower than those calculated by conventional design approaches. Meanwhile, relevant studies (Bienen et al., 2025; Kazemi Esfeh et al., 2026; Saegusa et al., 2024) have reported divergent findings: piles installed by the vibro-driven method may exhibit comparable lateral resistance, higher vertical bearing capacity, or lower vertical bearing capacity compared to other installation methods. As such, the impact of the vibro-driven method on pile bearing characteristics remains inconclusive.

Table 1. Scaling laws.

Parameter	Unit	Scale factor
Gravitational acceleration, g	m/s^2	N
Dimension, *L*	m	1/N
Mass, *m*	kg	$1/N^3$
Frequency, *f*	Hz	N
Time, *T*	s	1/N

Therefore, this study investigates the bearing capacities of piles installed in centrifugal fields using both vibro-driven and static penetration methods. To evaluate the effectiveness of pile installation in centrifugal fields, piles installed in 1g fields were also tested for their bearing capacities in centrifugal fields for comparison. The soil condition inside the piles was also examined in all cases.

2 EXPERIMENTAL METHODS

2.1 Experimental apparatus and scaling laws

Centrifugal model tests were conducted using a beam-type centrifuge apparatus (owned by TOYO Construction Co., Ltd., Naruo Research Institute; effective radius: 2.2 m). Table 1 summarizes the similarity ratios relevant to this experiment. The centrifugal acceleration was set to 20g.

Table 2. Model and prototype conversion parameters.

Steel pipe pile			
Parameter	**Unit**	**Model**	**Prototype**
mass	kg	0.454	3632 (3.6t)
Outer diameter	mm	40	800
Inner diameter	mm	38	760
Thickness	mm	1	20
Length	mm	300	6000 (6m)

Vibro-driven device			
Parameter	**Unit**	**Model**	**Prototype**
mass	kg	6.470	51760 (51.8t)
Frequency	Hz	180	9
Amplitude	mm	0.3	6

The soil container was a cylindrical tank with an inner diameter of 390 mm and a height of 580 mm. A guide was attached on top to ensure vertical penetration of the model pile. The model pile, made of brass, had a mass of 0.454 kg, wall thickness of 1 mm, length of 300 mm, outer diameter of 40 mm, and inner diameter of 38 mm.

Given that scaling the frequency and amplitude of the vibro-driven according to similitude laws for the centrifugal field would result in high-frequency and very small amplitude, and that the vibration device must withstand substantial loads due to its own centrifugal force and penetration constraints in the soil, a robust vibration system was required. Therefore, a wall-type hand vibrator for concrete compaction (power supply: 100V) was used as a substitute for the model vibro-driven. The acceleration waveform during model pile installation at 20g using this vibro-driven is shown in Figure 1. The hand vibrator had a mass of 6.47 kg (its weight in 20g fields is 129.4 kgf (≈1.27 kN)), a vibration frequency of 180 Hz, and an amplitude of 0.3 mm. When converted to prototype scale, this corresponds to a vibro-driven with a mass of 51.8 t, a frequency of 9 Hz, and an amplitude of 6 mm. Table 2 presents the correspondence between model and prototype parameters.

The model ground consisted of a dry mixed sand, prepared by blending No. 6 silica sand (G_s = 2.64, D_{50} = 0.32 mm) and No. 7 silica sand (G_s = 2.64, D_{50} = 0.10 mm) at a ratio of 2:1. The particle size distribution and physical properties of the mixed sand are shown in Figure 2. The mixed sand was compacted in 10 cm lifts using a vibrator, resulting in a soil container with a height of 30 cm and relative density D_r = 100 % within the cylindrical container.

2.2 Experimental Method

Two penetration methods were employed for installing the model piles: vibro penetration and static penetration. For the vibro penetration tests, the model vibro-driven described above was connected to the model pile, and the pile was installed by the combined self-weight of the vibro-driven and the pile itself (see Figure 3). For static penetration, a loading apparatus equipped with a 2-ton load cell was used to apply a constant displacement rate of 1.2 mm/min (see Figure 4). Each device was independent and could be attached or removed from the top of the cylindrical soil container.

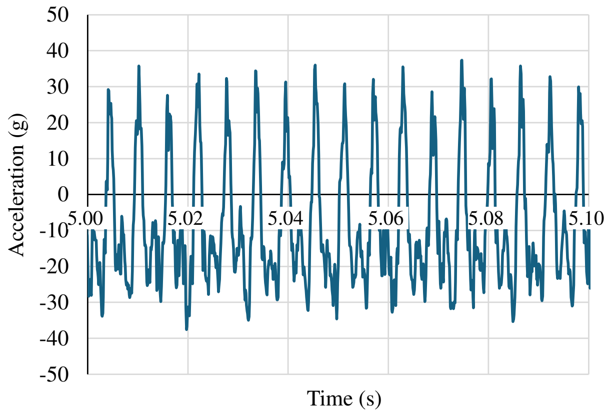

Figure 1. Acceleration during model pile driving using a vibro (g = 9.81 m/s²).

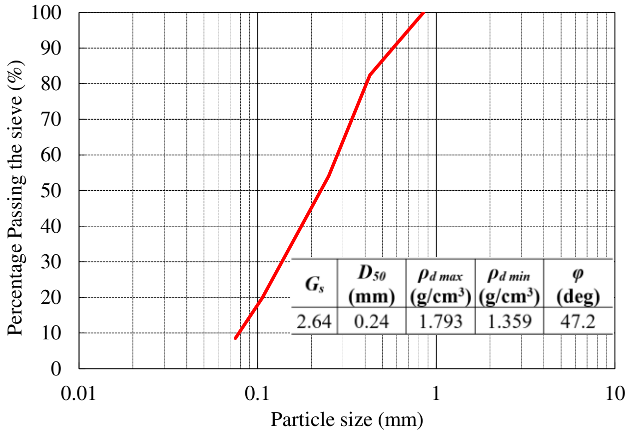

G_s	D_{50} (mm)	$\rho_{d\,max}$ (g/cm³)	$\rho_{d\,min}$ (g/cm³)	φ (deg)
2.64	0.24	1.793	1.359	47.2

Figure 2. Particle size distribution and physical properties of mixed sand.

Using these devices, piles were penetrated from the surface of the model ground to a depth of 100 mm under both 1g and centrifuge 20g conditions. Subsequently, in all tests, the bearing capacity tests were conducted to a depth of 110 mm under a 20g centrifugal field using a static penetration device. A schematic diagram of the experimental procedure is shown in Figure 5. The specific experimental cases are summarized in Table 3.

After measuring the penetration resistance in each case, the height and mass of the sand inside the model pile were measured to determine the dry density of the sand within the pile.

Table 3. Test cases.

Case	Penetration method and gravitational field	Centrifugal field for bearing capacity test (g)
1	Vibro_20G	20
2	Static_20G	20
3	Vibro_1G	20
4	Static_1G	20

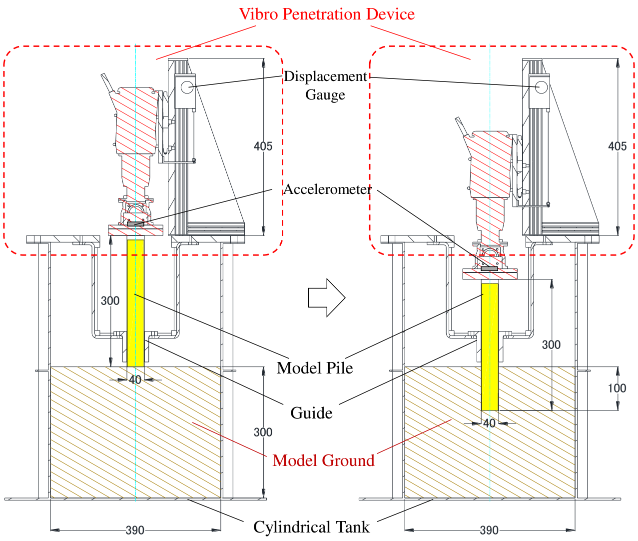

Figure 3. Vibro penetration device.

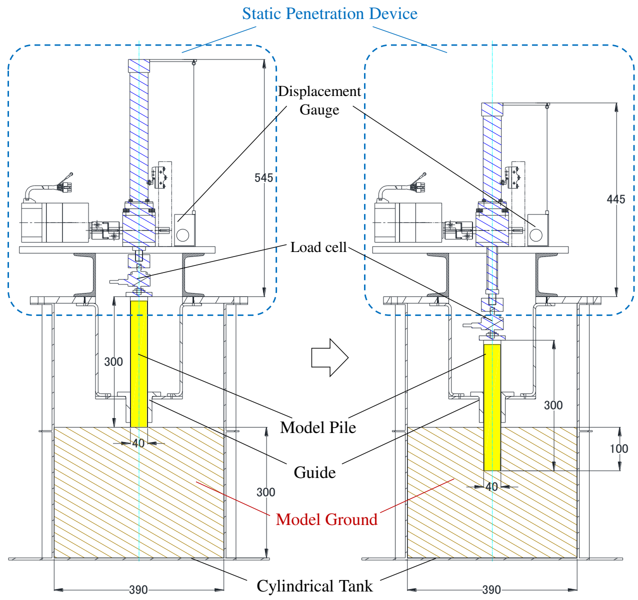

Figure 4. Static penetration device.

3 RESULTS

3.1 Penetration Velocity by Vibro Penetration

In Case 1, where vibro penetration was conducted under a centrifugal field of 20g, the pile penetrated 17 mm into the ground immediately after setting up the vibro penetration device under 1g conditions, due to

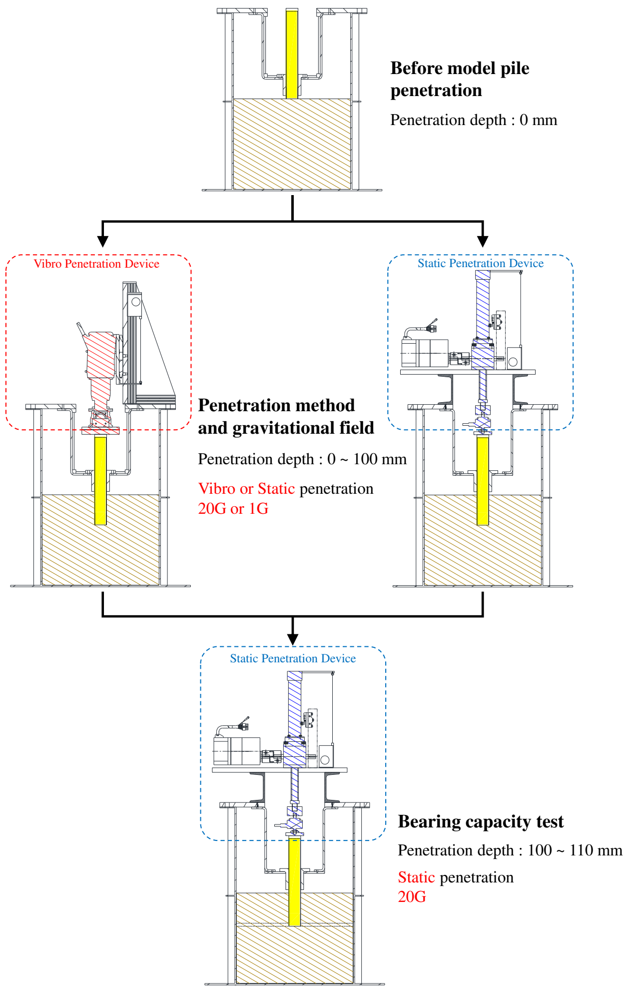

Figure 5. A schematic diagram of the experimental procedure.

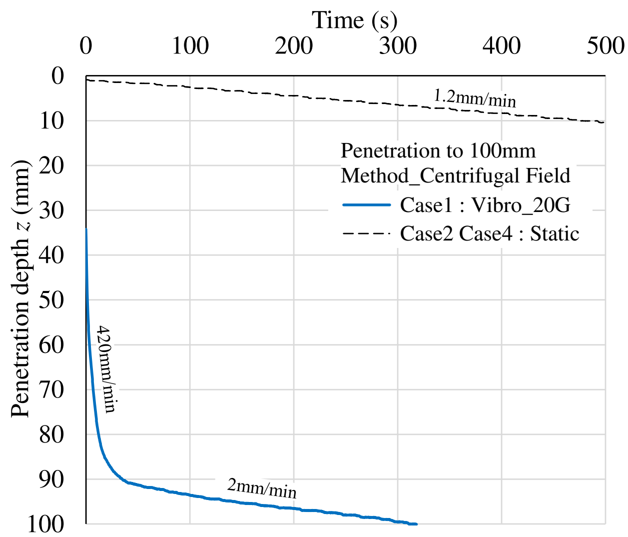

Figure 6. Relationship between penetration time and penetration depth during vibro-penetration in a 20g field (penetration velocity).

centrifugal field was increased to 20g using the centrifuge, the self-weight and the centrifugal force caused the pile to reach a penetration depth of 34 mm

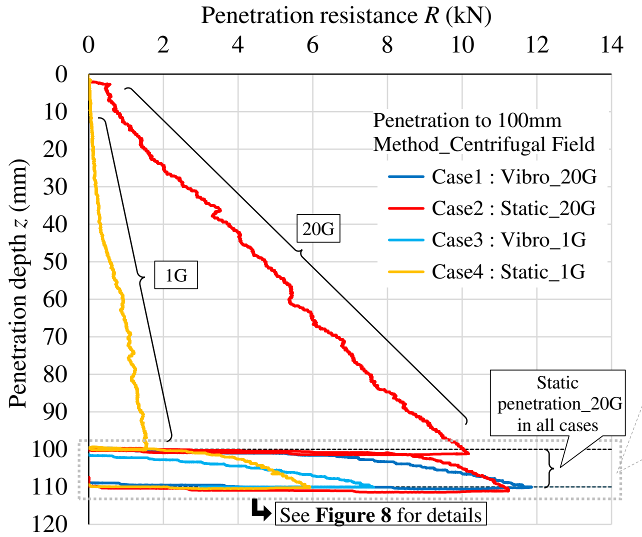

Figure 7. Relationship between penetration depth and penetration resistance (z = 0 ~ 100 mm).

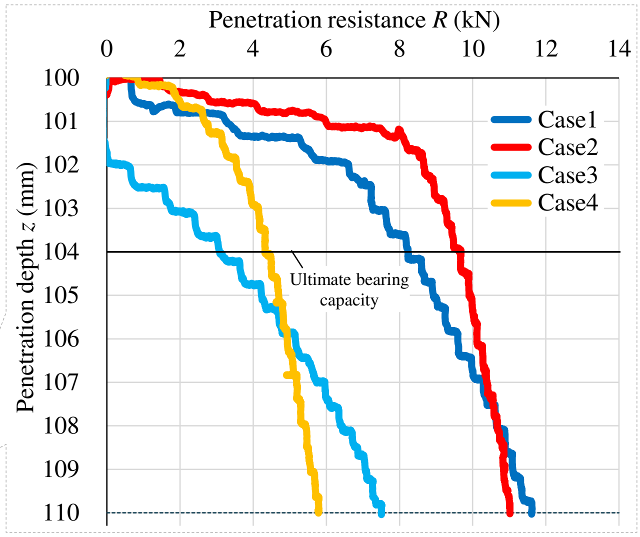

Figure 8. Relationship between penetration depth and penetration resistance (z = 100 ~ 110 mm).

from the ground surface. After activating the vibro-driven, the relationship between penetration depth and time until reaching a depth of 100 mm from the surface is shown in Figure 6. From the ground surface to a depth of 80 mm, the pile penetrated at an almost constant rate of approximately 420 mm/min. Between 80 mm and 90 mm, the penetration rate gradually decreased in a nonlinear fashion, and from 90 mm onwards, the pile advanced at a nearly constant slow rate of about 2 mm/min until reaching 100 mm. The total time required to reach 100 mm after starting the vibro-driven was 318 seconds.

On the other hand, for Case 3, where vibro penetration was performed under 1g conditions, the pile penetrated 17 mm due to the self-weight of the vibro-driven, similar to Case 1. Once the vibro-driven was activated, the pile rapidly advanced, and reached 100 mm depth in approximately 1 second.

For the static penetration tests (Cases 2 and 4), the penetration rate was maintained at 1.2 mm/min, so it took about 1.5 hours to reach 100 mm from the start of penetration.

3.2 Penetration Resistance in Each Case

The relationship between penetration depth and penetration resistance for each case is shown in Figure 7. To avoid damage to the load cell caused by vibrations, penetration resistance was not measured from the ground surface in the vibro penetration tests (Case 1 and Case 3). However, for the static penetration tests (Case 2 and Case 4), penetration resistance was recorded from the ground surface. In all cases, penetration resistance increased with greater penetration depth.

Figure 8 depicts the relationship between penetration resistance and penetration depth from 100 mm to 110 mm under a centrifugal field of 20g, using the static penetration method for all cases. In all cases, the penetration resistance rose sharply from the commencement of penetration, then transitioned to a more gradual increase.

Comparing cases where penetration was performed up to 100 mm under a 20g centrifugal field (Case 1 and Case 2) with those performed under a 1g field (Case 3 and Case 4), penetration resistance in the 20g field was approximately 1.5–2.0 times greater than in the 1g field. Differences were also observed in the dry density of the soil inside the model pile after penetration resistance measurements; further details are provided in subsequent sections.

For comparison between vibro and static penetration under 20g conditions (Case 1 and Case 2), the relationship between penetration depth and resistance was nearly identical. According to the Japanese Specifications for Highway Bridges (Japan Road Association, 2025), the ultimate bearing capacity is defined as either the load at which the load–displacement curve is nearly parallel to the displacement axis, or, if the displacement exceeds 10% of the pile diameter, the load at a displacement equal to 10% of the pile diameter. In this study, defining the ultimate bearing capacity as the load at 0.1D settlement resulted in a critical penetration depth of 104 mm. At this depth, the penetration resistance was lower for vibro penetration than for static penetration. However, as the penetration depth increased further, the penetration resistance in both methods became similar, indicating only a small effect of the penetration method. The reason for the lower penetration resistance in vibro penetration during the initial penetration stage is presumed to be the

Table 4. Soil height and dry density within the model pile.

Case	**1**	**2**	**3**	**4**
Dry density (g/cm^3)	1.742	1.731	1.692	1.696
Depth from the ground surface to the pile (mm)	6.5	2.5	1.0	1.5

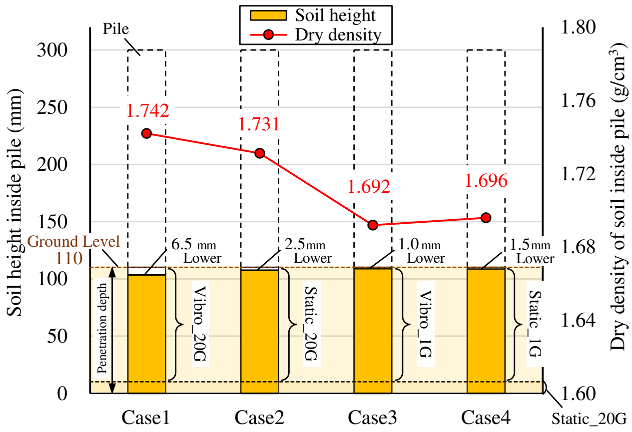

Figure 9. Graph of soil height and dry density in model piles.

Figure 10. Post-test condition inside the pile (Case 1).

disturbance of soil directly beneath the pile caused by vibrations.

In Case 3, only under 1g vibro penetration, penetration resistance was not observed in the range from 100 mm to 102 mm. This is thought to be due to the disturbance of the sand below the pile tip by vibration under the 1g field, so that when the field was subsequently switched to 20g by centrifugal loading, the model pile penetrated into the disturbed sand without resistance for about 2 mm due to its own weight.

3.3 Characteristics of the Soil Inside the Model Pile

After measuring penetration resistance in all cases, the height of the soil both inside and outside the model pile was recorded. The ground outside the pile was carefully excavated, and the soil inside the pile was extracted. The mass of the soil inside the model pile was measured to determine its dry density. Figure 9 and Table 4 show the height and dry density of the soil inside the pile.

The height of the soil inside the model pile was the lowest in Case 1 (vibro penetration under 20g), where it was 6.5 mm lower than the ground level outside the pile. In the other cases, the differences were minimal, generally within 1–2 mm. The dry density of the soil inside the pile was higher for penetration under 20g centrifugal acceleration (Case 1 and Case 2), compared to 1g condition (Case 3 and Case 4).

Additionally, for Case 1 and Case 2 (penetration under 20g), when extracting the model pile from the soil, it was observed—despite using dry sand—that the sand at the tip of the pile would fall out easily within the first 2 cm, but beyond that, the sand inside the pile was completely clogged and required multiple taps to be released, as shown in Figure 10. On the other hand, for Case 3 and Case 4 (penetration under 1g), all sand inside the pile was instantly released without clogging, clearly highlighting the visual difference in soil clogging between the cases.

These results suggest, as seen in Figure 8, that penetration resistance under 20g centrifugal acceleration was greater than under 1g, likely because the dry density of the soil inside the pile was higher and thus more easily clogged, resulting in an increased end bearing capacity. Therefore, penetration experiments under 1g may not accurately evaluate the bearing capacity of the model pile.

4 DISCUSSION

The reliability of the penetration resistance in both the 20g and 1g fields was verified by calculating the pile bearing capacity using theoretical equations. Based on the internal friction angle φ of the mixed sand used in the model ground, the pile penetration resistance R at a penetration depth of z = 104 mm was calculated using the following equations.

$$R = R_p + R_s \tag{1}$$

where R (kN) represents the penetration resistance, R_p (kN) denotes the tip resistance, R_s (kN) indicates the shaft resistance. The tip resistance R_p and shaft resistance R_s are calculated as follows:

$$R_p = N_q \cdot \sigma_{v0} \cdot A_p \tag{2}$$

$$R_s = K_s \cdot \sigma_{v0} \cdot \tan\delta \cdot A_s \tag{3}$$

where N_q is the bearing capacity factor, σ_{v0} (kN/m²) is the vertical stress, A_p (m²) is the core cross-sectional area of the pile, K_s is the lateral earth pressure

Table 5 Parameters used in theoretical value calculations.

Parameter	Unit	Value
φ	deg	47.2
δ	deg	31.6
z	mm	104
γ	kN/m^3	352
K_s	-	0.5
A_p	cm^2	12.6
A_s	cm^2	130.7
N_q	-	193.7

Table 6 Comparison of penetration resistance (R) at z = 104 mm with the theoretical value.

Theory and Measurement	Penetration resistance R (kN)
Theoretical Value	9.0 (R_p = 8.9, R_s = 0.07)
Case1_Vibro 20G	8.6
Case2_Static 20G	9.7
Case3_Vibro 1G	3.6
Case4_Static 1G	4.5

coefficient, δ (deg) is the friction angle between steel and mixed sand, and A_s (m²) is the shaft surface area of the pile. The bearing capacity factor N_q is calculated using Terzaghi's formula:

$$N_q = e^{\pi \tan\varphi} \cdot tan^2\left(45° + \frac{\varphi}{2}\right) \tag{4}$$

The parameters used for the theoretical calculations are listed in Table 5. It should be noted that the calculations were performed assuming centrifugal acceleration of 20g (20 × 9.81 m/s²). Table 6 compares the theoretical penetration resistance R at z = 104 mm with the experimental values obtained from Figure 8 for each case. The theoretical value was R = 9.0 kN, which closely matched the values measured for the cases penetrated under the 20g centrifugal field using both vibro and static penetration methods. This suggests that penetration testing under centrifugal acceleration is effective for evaluating the bearing capacity of piles under realistic stress conditions. However, in this experiment, the mixed sand was graded and compacted to achieve a very high density, resulting in an exceptionally large internal friction angle φ and, consequently, a large bearing capacity factor N_q. The penetration resistance R depends strongly on the bearing capacity factor N_q.Although the internal friction angle φ was accurately determined by direct shear tests, if φ varies by ±1°, the penetration resistance R changes by approximately 20%. Future studies should carefully consider the calculation of theoretical values as well as boundary conditions of the container.

5 CONCLUSIONS

In this study, model piles were installed using both the vibro-driven method and static penetration under 1g and centrifugal acceleration fields. The effects of gravity conditions and penetration methods on the penetration resistance and dry density of soil within the model piles were investigated. The main findings are summarized as follows:

- In this study, our main focus was to investigate the relationship between soil plugging behavior inside the model pile and its bearing capacity. Therefore, when designing the model pile, we prioritized factors such as pile wall thickness, sand grain size, and testing under a centrifuge condition. As a result, the model pile size was fixed, and due to limitations in the platform size of our company's centrifuge facility, the diameter of the soil container was constrained, resulting in a relatively small container-to-pile diameter ratio. We acknowledge that this could have caused boundary effects that may influence stress distribution and vibration propagation.

  In future studies, we plan to reduce these possible boundary effects by increasing the container size in relation to the pile, either by downsizing the model pile or improving the centrifuge facility to accommodate a larger soil container.
- Penetration resistance was higher under 20g centrifugal field compared to 1g, and this increase correlated with higher dry density of the soil within the model pile. The penetration resistance under the 20g condition was close to the theoretical bearing capacity; thus, model pile tests under real stress using a centrifuge apparatus may be an effective method for evaluating full-scale bearing capacity.
- Comparison of vibro penetration and static penetration revealed that vibro penetration resulted in lower penetration resistance in shallow ground due to vibration effects. However, once the pile reached a depth where vibration had negligible influence, the penetration resistance for both methods became almost identical.

Future challenges and considerations are as follows:

- In these experiments, a simple vibrating device was used as a substitute for a vibro driven; however, real vibro drivens for steel pile installation generate vertical vibrations with accurate sinusoidal waveforms. Therefore, improving the precision of the vibro model is needed.

In addition, because the performance of the vibro-driving method is highly dependent on the soil density, the present experiments were limited to high-density sand. In future studies, we will also investigate loose and medium-density sands to clarify how vibro-driving behavior changes with different ground conditions.

- Evaluation of bearing capacity in layered soils and different soil types, such as clay, to better reflect actual field conditions.
- Establishment of measurement methods to separately quantify shaft friction and tip resistance.
- In this study, the degree of soil plugging was evaluated based on the post-test measurements of the soil height and dry density inside the pile, as well as visual observations. In future work, we plan to design the experimental apparatus to allow for measurement of the time-dependent variation of soil height inside the model pile during installation and bearing capacity tests, so that the incremental filling ratio can be directly monitored.
- While this study compared vibro and static penetration, practical alternatives to the vibro method include impact methods such as hydraulic hammers. Verification of penetration resistance for impact installation methods under centrifugal acceleration is also required.

REFERENCES

Bienen, B., Mazutti, J.H., Bransby, M.F., Randolph, M.F., Peccin da Silva, A., Post, M., and Elkadi, A.S.K. (2025) *Physical modelling of vibro-driven piles in sand.* ISFOG2025, ISSMGE

Fetrati, M., Goodarzi, M., Ghasemi, P., Kreiter, S., Herwig, V., and Coronel Uriona, M. (2025). *Back analysis of driving resistance and induced driving stresses in vibratory driven XL monopiles: Case study of Kaskasi Wind Park.* ISFOG2025, Nantes, France.

Japan Road Association (2025). *Specifications for Highway Bridges, Part VI: Substructures.* Tokyo: Japan Road Association. (in Japanese)

Kazemi Esfeh, P., Bienen, B., Bransby, M.F., and Staubach, P. (2026) *Insights into pile vibro-driving in sand through numerical modelling.* Computers and Geotechnics, 189, 107628.

Saegusa, R., Kikuchi, Y., and Ishimaru, T. (2024). *Bearing capacity of steel pipe pile installed by vibro-hammer method.* Journal of Japan Society of Civil Engineers, 80(18), 24-18103. (in Japanese)

Vibro Hammer Method Technology Study Group (2024) *Design and construction manual of vibro hammer.* (in Japanese)